Nodal variational principle for excited states

Federico Zahariev, Mark S. Gordon, and Mel Levy

Phys. Rev. A **98**, 012144 — Published 31 July 2018

DOI: 10.1103/PhysRevA.98.012144

Nodal Variational Principle for Excited States

Federico Zahariev[1*], Mark S. Gordon[1†], and Mel Levy[2,3,4‡]

1. Department of Chemistry and Ames Laboratory, Iowa State University, Ames, Iowa 50011, USA
2. Department of Chemistry, Duke University, Durham, North Carolina 27708, USA
3. Department of Physics, North Carolina A&T State University, Greensboro, North Carolina 27411, USA
4. Department of Chemistry and Quantum Theory Group, Tulane University, New Orleans, Louisiana 70118, USA

June 8, 2018

It is proven that the exact excited-state wavefunction and energy may be obtained by minimizing the energy expectation value of trial wavefunctions that are constrained only to have the correct nodes of the state of interest. This excited-state nodal minimum principle has the advantage that it requires neither minimization with the constraint of wavefunction orthogonality to all lower eigenstates nor the antisymmetry of the trial wavefunctions. It is also found that the minimization over the entire space can be partitioned into several interconnected minimizations within the individual nodal regions, and the exact excited-state energy may be obtained by a minimization in just one or several of these nodal regions. For the proofs of the theorem, it is observed that the many-electron eigenfunction (excited state as well as ground state), restricted to a nodal region, is equivalent to a ground state wavefunction of one electron in a higher dimensional space; and an explicit excited-state energy variational expression is utilized by generalizing the Jacobi method of multiplicative variation. In corollaries, error functions are constructed for cases for which the nodes are not necessarily exact. The exact nodes minimize the energy error functions with respect to nodal variations.

I. INTRODUCTION

Variational principles have provided the most popular and effective ways to compute the properties of electronic systems. In this connection, it is well known that the minimization of the

* fzahari@iastate.edu
† mark@si.msg.chem.iastate.edu
‡ mlevy@tulane.edu

expectation value of the Hamiltonian yields the wavefunction and energy of the k^{th} eigenstate if the trial wavefunction for the k^{th} state is constrained to be orthogonal to the wavefunctions for the 0, 1, 2, …, k-1 states, where the energy of state n+1 is understood to be at least as high as the energy of state n. A related notion is the Hylleraas-Undheim-MacDonald theorem [1]. This theorem states that the eigenvalues of the Hamiltonian matrix in any finite dimensional subspace of the Hilbert space are bounded from below by the true eigenvalues of the Hamiltonian. High quality results typically require relatively large finite dimensional subspaces, where the eigenvalue problem becomes computationally expensive. In fact, the computational cost of the best eigenvalue solver algorithms scale quadratically with the dimension of the subspace.

With this in mind, it is the purpose of this paper to present a nodal variational principle for excited states. Specifically, we prove that in order to obtain the energy and wavefunction of the k^{th} state it is sufficient that the minimization takes place with the constraint that the trial wavefunction has the same nodes as the wavefunction of the k^{th} eigenstate. It is not necessary to impose the difficult orthogonality constraint. It is also not necessary to impose explicitly antisymmetry. The imposition of the nodal constraint is sufficient.

While interest in nodes of eigenfunctions goes back at least to the proof that the k^{th} eigenfunction of the one-electron Schrödinger equation, in any multi-dimensional space, has no more than k nodal regions [2], and although research regarding nodes and their properties continued [3], it was the ground-state fixed-node variational principle [4] and tiling theorem [5] of the Quantum Monte Carlo (QMC) method that aroused substantial interest in nodes and their properties [6-11]. The ground-state fixed-node variational principle states that an energy minimization in a nodal region of an arbitrary antisymmetric wavefunction gives an upper bound to the ground-state energy, and if a nodal region is bounded by the exact nodes, the energy minimization gives the ground-state energy. The proof of the ground-state fixed-node variational principle indirectly relies on the tiling theorem [5].

The QMC method is now being commonly used for excited states as well as ground states. In fact, the nodal variational principle for excited states presented in this paper is being implied *without a proof* for a number of QMC applications, such as the computations of optical gaps in nanostructures [12] and solids [13], diffusive properties of the vacancy defects in diamond [14], diamonoid excitation energies and Stokes shifts [15], excitation spectra of localized Wigner

states [16], quasi-particle excitations of the electron gas [17], and electronic [18] and rovabrational excitations [19] of molecules. As the QMC experience demonstrates, even approximations to the correct nodal surfaces typically result in accurate excited-state values.

The ground-state fixed-node variational principle has been extended to non-degenerate [6] and degenerate [7] excited states that are ground states within certain symmetry classes of trial wavefunctions. More precisely, the trial wavefunctions are supposed to transform according to the one-dimensional irreducible representation of the symmetry point group of the Hamiltonian. The proofs that are used therein are symmetry-restricted generalizations of the ground-state fixed-node proof [4] and rely on symmetry-restricted generalizations of the ground-state tiling theorem [5]. Although symmetries are not uncommon in molecules consisting of a handful of atoms, larger molecules are less likely to posses any symmetry, and no tiling theorem currently exists that would be applicable to an arbitrary excited state. In contrast, the proofs of the theorem, its corollaries, and the supporting lemma in the current paper do not rely on a tiling theorem and are applicable to any excited state.

We prove the theorem and its corollaries by means of two complementary routes, A and B. Proof A is based on our observation that a many-electron wavefunction, with a domain of consideration that focuses upon a single nodal region, is equivalent to a single-electron wavefunction in a higher dimensional space. Proof B extends the ground-state Jacobi method of multiplicative variation to excited states.

Moreover, when the exact nodes are not known, corollaries to the proofs given here construct two different error functions that assess the quality of approximate nodes. These error functions incorporate energy minimization with the given approximate nodes. The minimization of the error functions, with respect to variations of the nodes, achieves zero once the geometries of the nodes become exact. We show that the explicit antisymmetry constraint is not necessary even when the nodes are approximate. Numerical examples illustrate the use of the error functions.

II. NODAL VARIATIONAL PRINCIPLE

Given below are the two different proofs of our *theorem* that expresses the following nodal variational principle for excited states:

(i) *The minimum of the energy expectation value of trial wavefunctions that are analytically well behaved and have the nodes of the exact eigenfunction* $\Psi_k\left(\boldsymbol{r}_1,\boldsymbol{r}_2,...,\boldsymbol{r}_N\right)$ *of N-electrons is the exact eigenvalue* E_k. *The minimum of the energy expectation value is achieved at the exact eigenfunction* $\Psi_k\left(\boldsymbol{r}_1,\boldsymbol{r}_2,...,\boldsymbol{r}_N\right)$.

(ii) *In addition, even the minimization in just one or several nodal regions also yields* E_k.

Note that it has been shown [20, 21] that spin-free wave functions are sufficient in the context of the present work.

III. PROOFS OF THE THEOREM

Proof A: Consider the nodal hypersurface corresponding to the k-th eigenfunction; i.e. all of the points in the 3N-dimensional coordinate space of N electrons that satisfy the condition $\Psi_k\left(\boldsymbol{r}_1,\boldsymbol{r}_2,...,\boldsymbol{r}_N\right)=0$. This nodal hypersurface, i.e. a (3N-1)-dimensional surface in the 3N-dimensional space of electron positions, partitions the configuration space into m nodal regions L_j $\left(j=1,2,\ldots,m\right)$. $\Psi_k\left(\boldsymbol{r}_1,\boldsymbol{r}_2,...,\boldsymbol{r}_N\right)$ is either strictly positive or strictly negative in each of the m nodal regions. Some technical aspects of the nodal constraint are in Appendix I of the Supplementary Material.

Now consider a trial wavefunction $\Psi^{(k)}\left(\boldsymbol{r}_1,\boldsymbol{r}_2,...,\boldsymbol{r}_N\right)$ that is not necessarily antisymmetric with respect to the exchange of like-spin electrons and has the same nodes as the k-th eigenfunction $\Psi_k\left(\boldsymbol{r}_1,\boldsymbol{r}_2,...,\boldsymbol{r}_N\right)$. The trial wavefunction $\Psi^{(k)}\left(\boldsymbol{r}_1,\boldsymbol{r}_2,...,\boldsymbol{r}_N\right)$, which is normalized to unity, could be the exact k-th eigenfunction $\Psi_k\left(\boldsymbol{r}_1,\boldsymbol{r}_2,...,\boldsymbol{r}_N\right)$ itself. The integration over the entire 3N-dimensional space can be partitioned into a sum of integrations over the m nodal regions,

$$\left\langle \Psi^{(k)} \middle| \Psi^{(k)} \right\rangle = \sum_{j=1}^{m} \left\langle \Psi^{(k)} \middle| \Psi^{(k)} \right\rangle_{L_j} = \sum_{j=1}^{m} p_{L_j} = 1, \qquad (1)$$

where $\left\langle \Psi^{(k)} \middle| \Psi^{(k)} \right\rangle_{L_j}$ signifies $\left\langle \Psi^{(k)} \middle| \Psi^{(k)} \right\rangle$ in the nodal region L_j.

The energy expectation value of $\Psi^{(k)}\left(\boldsymbol{r}_1, \boldsymbol{r}_2, ..., \boldsymbol{r}_N\right)$ can be similarly partitioned as

$$E^{(k)} = \left\langle \Psi^{(k)} \middle| \hat{H} \middle| \Psi^{(k)} \right\rangle = \sum_{j=1}^{m} \left\langle \Psi^{(k)} \middle| \hat{H} \middle| \Psi^{(k)} \right\rangle_{L_j} = \sum_{j=1}^{m} \left\langle \Psi^{(k)} \middle| \Psi^{(k)} \right\rangle_{L_j} \frac{\left\langle \Psi^{(k)} \middle| \hat{H} \middle| \Psi^{(k)} \right\rangle_{L_j}}{\left\langle \Psi^{(k)} \middle| \Psi^{(k)} \right\rangle_{L_j}}. \qquad (2)$$

The expressions $\dfrac{\left\langle \Psi^{(k)} \middle| \hat{H} \middle| \Psi^{(k)} \right\rangle_{L_j}}{\left\langle \Psi^{(k)} \middle| \Psi^{(k)} \right\rangle_{L_j}}$, which we now denote as $E_{L_j}^{(k)}$, on the right-hand side of Eq. (2) are the energy expectation values of $\Psi^{(k)}\left(\boldsymbol{r}_1, \boldsymbol{r}_2, ..., \boldsymbol{r}_N\right)$ in the individual nodal regions L_j and $p_{L_j} = \left\langle \Psi^{(k)} \middle| \Psi^{(k)} \right\rangle_{L_j}$ is the respective probability of finding the N-electron system in the individual nodal region L_j. Consequently, the right-hand side of Eq. (2) is an average over the nodal-region energies that are weighted by the respective probabilities. If the trial wavefunction $\Psi^{(k)}\left(\boldsymbol{r}_1, \boldsymbol{r}_2, ..., \boldsymbol{r}_N\right)$ is the exact eigenfunction $\Psi_k\left(\boldsymbol{r}_1, \boldsymbol{r}_2, ..., \boldsymbol{r}_N\right)$ itself, then $E_{L_j}^{(k)} = E^{(k)} = E_k$. (A similar partitioning of the energy expectation value of a one-dimensional Hamiltonian was used in Ref. [11] in the proof of a different variational principle involving nodes.)

It is important to observe here that the k-th eigenfunction $\Psi_k\left(\boldsymbol{r}_1, \boldsymbol{r}_2, ..., \boldsymbol{r}_N\right)$ in a nodal region is, in fact, the ground-state solution for the given nodal region. This is because an eigenfunction that is either strictly positive or strictly negative is a ground state according to an extension presented here of a theorem of Courant and Hilbert [2]. Although the original theorem is for a one-electron wavefunction in a space of arbitrary dimension, *the many-electron*

eigenfunction $\Psi_k\left(\boldsymbol{r}_1,\boldsymbol{r}_2,...,\boldsymbol{r}_N\right)$*, restricted to a nodal region, can be equivalently interpreted as a ground state wavefunction of one electron in 3N-dimensional space*, *even when* $\Psi_k\left(\boldsymbol{r}_1,\boldsymbol{r}_2,...,\boldsymbol{r}_N\right)$ *is an excited state*.[§] In such an interpretation, the many-electron Hamiltonian is regarded as an effective Hamiltonian of one electron in 3N-dimensional space. The eigenfunction $\Psi_k\left(\boldsymbol{r}_1,\boldsymbol{r}_2,...,\boldsymbol{r}_N\right)$ may also be regarded as an eigenfunction of one electron in 3N-dimensional space.

According to the foregoing ground state minimum principle for each nodal region, the nodal region normalized energy expectation value of $\Psi^{(k)}\left(\boldsymbol{r}_1,\boldsymbol{r}_2,...,\boldsymbol{r}_N\right)$ cannot be lower than the nodal region normalized energy expectation value of the k-th eigenvalue of $\Psi_k\left(\boldsymbol{r}_1,\boldsymbol{r}_2,...,\boldsymbol{r}_N\right)$:

$$E_{L_j}^{(k)}=\frac{\left\langle\Psi^{(k)}\middle|\hat{H}\middle|\Psi^{(k)}\right\rangle_{L_j}}{\left\langle\Psi^{(k)}\middle|\Psi^{(k)}\right\rangle_{L_j}}\geq\frac{\left\langle\Psi_k\middle|\hat{H}\middle|\Psi_k\right\rangle_{L_j}}{\left\langle\Psi_k\middle|\Psi_k\right\rangle_{L_j}}=E_k\,. \tag{3}$$

Multiplication on both sides of the inequality in Eq. (3) by p_{L_j} followed by a summation over j gives

$$E^{(k)}=\left\langle\Psi^{(k)}\middle|\hat{H}\middle|\Psi^{(k)}\right\rangle=\sum_{j=1}^{m}p_{L_j}E_{L_j}^{(k)}\geq\sum_{j=1}^{m}p_{L_j}E_k=\left(\sum_{j=1}^{m}p_{L_j}\right)E_k=E_k\,, \tag{4}$$

[§] Note that the interchange symmetry of $\Psi_k\left(\boldsymbol{r}_1,\boldsymbol{r}_2,...,\boldsymbol{r}_N\right)$ does not play a role for an isolated nodal region for the following reason. If $\boldsymbol{r}_1,\boldsymbol{r}_2,...,\boldsymbol{r}_i,...,\boldsymbol{r}_j,...,\boldsymbol{r}_N$ belongs to a nodal region, then $\boldsymbol{r}_1,\boldsymbol{r}_2,...,\boldsymbol{r}_j,...,\boldsymbol{r}_i,...,\boldsymbol{r}_N$, in which the spatial coordinates corresponding to two spin-equivalent electrons are interchanged, is outside the nodal region, as the interchange changes the sign of the wavefunction.

The inequality in (4) arises because each p_{L_j} is non-negative, the use of normalization expression in Eq. (1), and the fact that the weighted average increases if any of the contributing energies increases. Eq. (4) proves part (i) of the theorem.

Eq. (3) demonstrates that an energy minimization in an isolated nodal region actually gives the exact energy E_k of the entire eigenfunction $\Psi_k\left(\boldsymbol{r}_1,\boldsymbol{r}_2,...,\boldsymbol{r}_N\right)$. More generally, consider an energy minimization over some of the nodal regions, such as over an isolated region of space bounded by nodes. An appropriately normalized nodal energy minimization over just some of the nodal regions also yields the exact energy E_k, as demonstrated by a generalization of Eq. (4):

$$\frac{\sum_j p_{L_j} E_{L_j}^{(k)}}{\sum_j p_{L_j}} \geq \frac{\sum_j p_{L_j} E_k}{\sum_j p_{L_j}} = E_k \ , \qquad (5)$$

where the partial sum is only over those nodes that participate in the minimization. Eq. (5) proves part (ii) of the theorem.

Proof B:

Consider trial wavefunctions of the type $g\left(\boldsymbol{r}_1,\boldsymbol{r}_2,...,\boldsymbol{r}_N\right)\Psi_k\left(\boldsymbol{r}_1,\boldsymbol{r}_2,...,\boldsymbol{r}_N\right)$, where the k$^{\text{th}}$ state $\Psi_k\left(\boldsymbol{r}_1,\boldsymbol{r}_2,...,\boldsymbol{r}_N\right)$ is kept fixed and the function $g\left(\boldsymbol{r}_1,\boldsymbol{r}_2,...,\boldsymbol{r}_N\right)$ is varied. The function $g\left(\boldsymbol{r}_1,\boldsymbol{r}_2,...,\boldsymbol{r}_N\right)$ is assumed to be everywhere smooth (in particular, everywhere finite) and such that $g\left(\boldsymbol{r}_1,\boldsymbol{r}_2,...,\boldsymbol{r}_N\right)\Psi_k\left(\boldsymbol{r}_1,\boldsymbol{r}_2,...,\boldsymbol{r}_N\right)$ is a well-behaved wavefunction. It is important to note that $g\left(\boldsymbol{r}_1,\boldsymbol{r}_2,...,\boldsymbol{r}_N\right)\Psi_k\left(\boldsymbol{r}_1,\boldsymbol{r}_2,...,\boldsymbol{r}_N\right)$ is not assumed here to be necessarily antisymmetric with respect to the exchange of like-spin electrons.

The theorem will now be proven by showing that the explicit form of the g-variations around the excited state $\Psi_k\left(\boldsymbol{r}_1,\boldsymbol{r}_2,...,\boldsymbol{r}_N\right)$, which can be considered to be a generalization to excited states of the Jacobi method of multiplicative variation**, is

$$\frac{\left\langle g\Psi_k\middle|\hat{H}\middle|g\Psi_k\right\rangle}{\left\langle g\Psi_k\middle|g\Psi_k\right\rangle}=E_k+\frac{\frac{1}{2}\sum_{i=1}^{N}\sum_{\alpha=x,y,z}\left\langle\left(\frac{\partial g}{\partial r_{i,\alpha}}\right)\Psi_k\middle|\left(\frac{\partial g}{\partial r_{i,\alpha}}\right)\Psi_k\right\rangle}{\left\langle g\Psi_k\middle|g\Psi_k\right\rangle}\geq E_k. \qquad (6)$$

Note that the inequality in Eq. (6) occurs because the sums are non-negative.

The equality on the left in Eq. (6) is derived by the following chain of equalities

$$\begin{aligned}
&\frac{\left\langle g\Psi_k\middle|\hat{H}\middle|g\Psi_k\right\rangle}{\left\langle g\Psi_k\middle|g\Psi_k\right\rangle}=\frac{\left\langle g\Psi_k\middle|\hat{T}\middle|g\Psi_k\right\rangle+\left\langle g\Psi_k\middle|\hat{V}\middle|g\Psi_k\right\rangle}{\left\langle g\Psi_k\middle|g\Psi_k\right\rangle}=\frac{\left\langle g\Psi_k\middle|\hat{T}\middle|g\Psi_k\right\rangle+\left\langle g^2\Psi_k\middle|\hat{V}\middle|\Psi_k\right\rangle}{\left\langle g\Psi_k\middle|g\Psi_k\right\rangle}\\
&=\frac{\left\langle g\Psi_k\middle|\hat{T}\middle|g\Psi_k\right\rangle+\left\langle g^2\Psi_k\middle|\left(\hat{H}-\hat{T}\right)\middle|\Psi_k\right\rangle}{\left\langle g\Psi_k\middle|g\Psi_k\right\rangle}=E_k+\frac{\left\langle g\Psi_k\middle|\hat{T}\middle|g\Psi_k\right\rangle-\left\langle g^2\Psi_k\middle|\hat{T}\middle|\Psi_k\right\rangle}{\left\langle g\Psi_k\middle|g\Psi_k\right\rangle}\\
&=E_k+\frac{\frac{1}{2}\sum_{i=1}^{N}\sum_{\alpha=x,y,z}\left\langle\left(\frac{\partial g}{\partial r_{i,\alpha}}\right)\Psi_k\middle|\left(\frac{\partial g}{\partial r_{i,\alpha}}\right)\Psi_k\right\rangle}{\left\langle g\Psi_k\middle|g\Psi_k\right\rangle}
\end{aligned} \qquad (7)$$

Additional details of the derivation of Eq. (7) can be found in Appendix II of the Supplementary Material.

At this stage, the inequality in Eq. (6) has been proved. But in order for the inequality to constitute a proof of the theorem, each trial wavefunction $\Psi^{(k)}\left(\boldsymbol{r}_1,\boldsymbol{r}_2,...,\boldsymbol{r}_N\right)$, that has the same nodes as the k-th eigenfunction $\Psi_k\left(\boldsymbol{r}_1,\boldsymbol{r}_2,...,\boldsymbol{r}_N\right)$, should be presentable as $g\left(\boldsymbol{r}_1,\boldsymbol{r}_2,...,\boldsymbol{r}_N\right)\Psi_k\left(\boldsymbol{r}_1,\boldsymbol{r}_2,...,\boldsymbol{r}_N\right)$. In other words, the well-behaved scaling function $g\left(\boldsymbol{r}_1,\boldsymbol{r}_2,...,\boldsymbol{r}_N\right)$

** On p. 458-459, Vol. I of [2] the Jacobi method of multiplicative variation is introduced and applied to the ground-state problem only.

must be presentable as $\frac{\Psi^{(k)}(\boldsymbol{r}_1,\boldsymbol{r}_2,...,\boldsymbol{r}_N)}{\Psi_k(\boldsymbol{r}_1,\boldsymbol{r}_2,...,\boldsymbol{r}_N)}$. Since $\Psi_k(\boldsymbol{r}_1,\boldsymbol{r}_2,...,\boldsymbol{r}_N)$ vanishes at the nodes, the finiteness of the ratio may not appear to be guaranteed. However, the ratio is in fact finite as shown in Appendix III of the Supplementary Material.

Thus, the inequality in Eq. (6), together with the fact that each trial wavefunction $\Psi^{(k)}(\boldsymbol{r}_1,\boldsymbol{r}_2,...,\boldsymbol{r}_N)$ that has the same nodes as the k-th eigenfunction $\Psi_k(\boldsymbol{r}_1,\boldsymbol{r}_2,...,\boldsymbol{r}_N)$ is presentable as $g(\boldsymbol{r}_1,\boldsymbol{r}_2,...,\boldsymbol{r}_N)\Psi_k(\boldsymbol{r}_1,\boldsymbol{r}_2,...,\boldsymbol{r}_N)$, proves part (i) of the theorem.

As with Proof A, Proof B can be adapted to a single nodal region, or more generally, to several nodal regions with an appropriate normalization of the energy expectation value. Eq. (6) implies that the analog of Eq. (5) is

$$\frac{\sum_j \langle g\Psi_k | \hat{H} | g\Psi_k \rangle_{L_j}}{\sum_j \langle g\Psi_k | g\Psi_k \rangle_{L_j}} = E_k + \frac{\frac{1}{2}\sum_j \sum_{i=1}^{N} \sum_{\alpha=x,y,z} \left\langle \left(\frac{\partial g}{\partial r_{i,\alpha}}\right)\Psi_k \middle| \left(\frac{\partial g}{\partial r_{i,\alpha}}\right)\Psi_k \right\rangle_{L_j}}{\sum_j \langle g\Psi_k | g\Psi_k \rangle_{L_j}} \geq E_k , \qquad (8)$$

where each sum in j could be replaced by simply one term when only one nodal region is used, which proves part (ii) of the theorem.

IV. COROLLARIES TO THE THEOREM

Now assume that the m nodal regions $\tilde{L}_j$ $(j=1,2,\ldots,m)$ are not necessarily the exact nodes of Ψ_k. It is assumed that the approximate nodes are variations around the exact ones, i.e. that the approximate nodes can be continuously deformed back to the exact ones.

In this case, the minimizing energies within the different nodal regions,

$$\tilde{E}^{(k)}_{\tilde{L}_j,\min} = \frac{\left\langle \tilde{\Psi}^{(k)}_{\min} \middle| \hat{H} \middle| \tilde{\Psi}^{(k)}_{\min} \right\rangle_{\tilde{L}_j}}{\left\langle \tilde{\Psi}^{(k)}_{\min} \middle| \tilde{\Psi}^{(k)}_{\min} \right\rangle_{\tilde{L}_j}} , \qquad (9)$$

may differ from each other. Although the trial wavefunctions $\tilde{\Psi}^{(k)}$ are not *constrained* to be antisymmetric, the energy-minimizing trial wavefunction $\tilde{\Psi}^{(k)}_{\min}$ will always be antisymmetric if the nodes come from *some* antisymmetric wavefunction, as the Lemma and its proof in Appendix IV of the Supplementary Material demonstrate.

A relevant "error expression", corresponding to $\tilde{\Psi}^{(k)}_{\min}$, is

$$\sum_{j=1}^{m}\left[\tilde{E}^{(k)}_{\tilde{L}_j \min}-\tilde{E}^{(k)}_{\min}\right]^2\left\langle\tilde{\Psi}^{(k)}_{\min}\middle|\tilde{\Psi}^{(k)}_{\min}\right\rangle_{\tilde{L}_j}, \qquad (10)$$

where

$$\tilde{E}^{(k)}_{\min}=\left\langle\tilde{\Psi}^{(k)}_{\min}\middle|\hat{H}\middle|\tilde{\Psi}^{(k)}_{\min}\right\rangle=\sum_{j=1}^{m}\tilde{E}^{(k)}_{\tilde{L}_j,\min}\left\langle\tilde{\Psi}^{(k)}_{\min}\middle|\tilde{\Psi}^{(k)}_{\min}\right\rangle_{\tilde{L}_j}. \qquad (11)$$

Note that the larger nodal regions are weighted higher in expression (10). This error expression achieves its minimum of zero if and only if the trial wavefunction $\tilde{\Psi}^{(k)}_{\min}$ is the true eigenfunction Ψ_k, because then all the nodal-region minimizing energies in Eq. (9) are equal.

Corollary I to the Theorem: The minimization of error expression (10), with respect to nodal variations, yields the correct nodes of Ψ_k.

Another nodal error expression is dictated by the use of $g\Psi_k$ in Proof B. The expression is

$$\left[\frac{\left\langle g\tilde{\Psi}_{\min}^{(k)}\middle|\hat{H}\middle|\tilde{\Psi}_{\min}^{(k)}\right\rangle}{\left\langle g\tilde{\Psi}_{\min}^{(k)}\middle|\tilde{\Psi}_{\min}^{(k)}\right\rangle}-\left\langle\tilde{\Psi}_{\min}^{(k)}\middle|\hat{H}\middle|\tilde{\Psi}_{\min}^{(k)}\right\rangle\right]^2. \qquad (12)$$

Corollary II to the Theorem: Minimization of error expression (12) with respect to nodal variations, for all allowable scaling functions g, yields the correct nodes of Ψ_k. Note that the allowable g's from Proof B are such that $g\tilde{\Psi}_{\min}^{(k)}$ preserves the nodes of $\tilde{\Psi}_{\min}^{(k)}$.

V. SIMPLE NUMERICAL EXAMPLES

It was observed earlier that a many-electron wavefunction, with a domain of consideration that is restricted to a single nodal region, is equivalent to a single-electron wavefunction in a higher dimensional space. As a result, a single-electron example is worthwhile for demonstrating the qualitative features of approximate nodal regions. As an illustration, consider the exact and approximate 4S state of the hydrogen atom. The approximate wavefunctions minimize the total energy while being constrained to approximate nodes. Tables V.1-V.4 in the Supplementary Material give data for four approximate wave functions that possess inexact nodes. The utility of error expression (10) for helping to select the best wavefunction is reflected in the fact that the wavefunction with the best average energy, which is associated with the bottom row of Table V.3, is the one that gives the lowest value for error expression (10); compare the bottom rows of Table V.1-V.4. Comparison of the bottom rows in Table V.1 and Table V.4 also reveals, however, that it is possible for a wavefunction with a higher value for error expression (10) to actually give a better average energy.

The green (middle) lines on the right-hand side of Fig. 1 [23], which is associated with the wavefunction in Table V.1, depict the nodal-region energy minima (solid lines) and actual eigenvalue (dotted line) of the example. The ground-state energies in the different approximate nodal regions are not necessarily equal, making the energy discontinuous across the nodes.

The right-hand side of Fig. 1 depicts the split of the nodal-region energies into their local kinetic and potential energy components, obtained by rearranging the eigenvalue equation as $\frac{-\frac{1}{2}\nabla^2\Psi(\vec{r})}{\Psi(\vec{r})}+V(\vec{r})=E$, which is the way it is utilized, for instance, in the familiar local energy and variance expressions [25, 26, 27]. As can be seen in Fig. 1, about the same nodal deviation from an exact nodal position can have a dramatically different impact on the nodal energy, depending on the strength of the external potential $V(\vec{r})$ at the position of a node. For this reason, energy based error expressions (10) and (12) give measures for gauging nodal quality that should provide worthwhile alternatives to the use of the geometric notion of nodal distance error [28, 29]. These energy-based error expressions measure the cumulative deviation of the nodal-region energy minima from the average energy. When the nodes are exact, all of these nodal-region energy minima equal the excited-state eigenvalue, which is a constant throughout the entire space.

It is interesting to note that the value of error expression (10) can be determined solely by the discontinuities of the local kinetic energy at the nodes. The value of error expression (10) is invariant with respect to a shift of all the nodal-region energy minima by the same constant and, as a result, this value depends only on the differences of the nodal-region energy minima. The differences of the neighboring nodal-region energy minima are, in turn, equivalent to the extent of the discontinuities of the local kinetic energy at the respective nodes.

If, through the use of error expressions (10) or (12), there is an indication that a particular subset of nodal regions might be preferred, then it would be reasonable to consider choosing this subset alone. For example, for the wavefunction associated with Table V.1, if only the third and fourth nodal regions (as counted from the nucleus outwards) are used, instead of all four nodal regions, the values of error expressions of Eq. (10) and Eq. (12) [30] go down from 1.0167×10^{-4} E_h^2 to 2.9484×10^{-7} E_h^2 and from 3.0694×10^{-3} E_h^2 to 7.9837×10^{-7} E_h^2, respectively, where E_h signifies the Hartree unit of energy. Simultaneously, the approximate energy estimate improves from -0.03139 E_h to -0.03126 E_h compared with the exact value of -0.03125 E_h. It becomes clear that a restriction to the third and fourth nodal regions of the approximate hydrogen atom 4S wavefunction improves the energy estimate. In fact, compared with all the nodal combinations in

Table V.1, the use of the third and fourth regions gives both the lowest value for error expression (10) and the best average energy. (When only a subset of the nodal regions is employed, for which zero values of error expressions 10 and 12 serve as necessary eigenstate conditions, it is understood that expressions 10, 11, and 12 are adjusted to incorporate the particular squares of the norms of the nodal regions.)

Appendix VI of the Supplementary Material contains two similar illustrative numerical examples based on the exact and approximate fifth excited states of the harmonic oscillator.

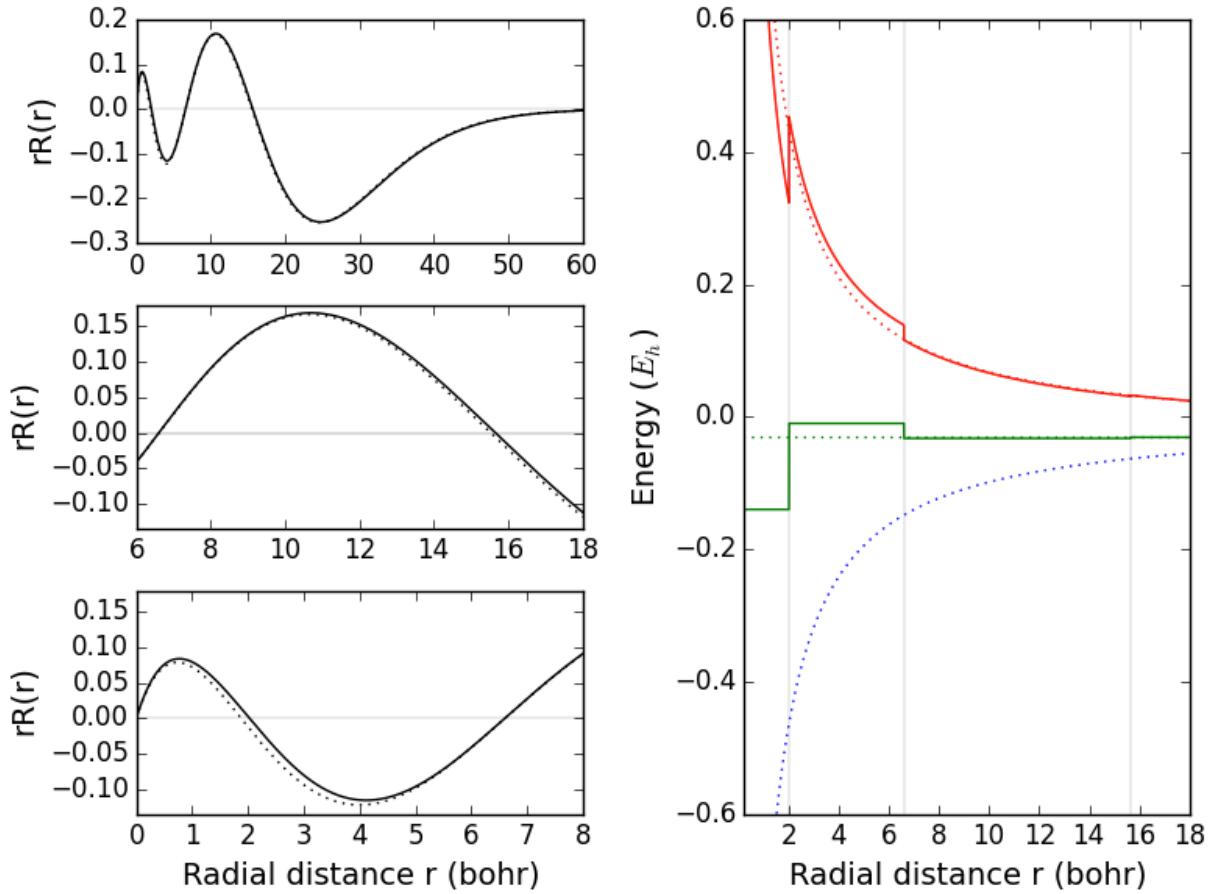

Fig. 1. The exact (dotted lines) and approximate (solid lines) wavefunctions corresponding to the 4S state of the hydrogen atom are depicted on the left-hand side of the figure on different radial distance scales. The exact wavefunction has nodes at r = 1.8716 bohr, 6.6108 bohr, and 15.5180 bohr, while the approximate wavefunction has nodes at 2.0240 bohr, 6.6068 bohr, and 15.6442

bohr. The four nodal regions are enumerated from the nucleus outwards. The exact energy of the hydrogen atom in the 4S state is -0.03125 E_h, while the nodal-region energies of the approximate hydrogen-atom wavefunction are -14.010×10^{-2} E_h (1^{st}), -1.000×10^{-2} E_h (2^{nd}), -3.261×10^{-2} E_h (3^{rd}), -3.106×10^{-2} E_h (4^{th}). The corresponding local energies are depicted on the right-hand side of the figure (kinetic: red (upper) curves; potential: blue (bottom) curve; total: green (middle) lines)

While the mathematical results in this paper are general, the difficulty is that their applications to many-electron systems require flexible and robust numerical representations of the multi-dimensional nodes. For these purposes, one might use generalizations of the approach in reference 31. In any case, our theorem justifies the interpretation that approximate excited state energies and wave functions are obtained even when the exact nodes are only known approximately, as exemplified by the cases given in the Introduction.

VI. CONCLUSIONS

In this paper, a minimum principle featuring nodes was proven for excited states. Aspects of this minimum principle are currently being actively utilized in practice, but no proof has actually been given until now.

The excited-state theorem within provides the realization that the minimization over the entire space can be partitioned into interconnected minimizations in individual exact nodal regions, and an energy minimization over all space or over one or several nodal regions gives the exact excited-state energy. Moreover, the exact excited-state wave function is obtained when the minimization is performed over all space. The smoothness of the trial wavefunctions across the nodes is the link between the minimizations within each of the nodal regions. Explicit expressions for the wavefunction variation around an excited state with the nodes constrained to the correct ones are given in Eq. (6) and Eq. (8).

Expressions (10) and (12) of the corollaries extend the minimum principle to nodal variations when the exact nodes are unknown. The lemma, proven in Appendix IV, supports the corollaries and establishes a key connection between the nodes and the antisymmetry of the trial wavefunctions.

The main results in this paper are formulated in the theorem and corollaries. In addition, we

have provided suggestions for calculations of excited states when approximate nodes are used in the nodal energy minimization process. With this in mind, simple numerical examples illustrate the use of expressions (10) and (12) as error estimates of approximate nodes.

It is expected that the excited state minimum principle presented here and the extension of the minimum principle to nodal variation, will have a wide range of new applications due to the general validity of these principles for excited states.

Acknowledgements: FZ and MSG are supported by the U.S. Department of Energy, Office of Basic Energy Sciences, Division of Chemical Sciences, Geosciences, and Biosciences, through the Ames Laboratory Chemical Physics program. The Ames Laboratory is operated for the U.S. Department of Energy by Iowa State University under Contract No. DE-AC02-07CH11358.

Appendix I

The nodal constraint is imposed by restricting the variational space to the linear space of wavefunctions that are well behaved and have the nodes of the k-th eigenfunction $\Psi_k\left(\boldsymbol{r}_1,\boldsymbol{r}_2,...,\boldsymbol{r}_N\right)$. In this Letter, a wavefunction is "well behaved" if it belongs to the space of "test functions" in the sense of the theory of tempered distributions, i.e. the wavefunction has partial derivatives of any order ("infinitely smooth") and falls off to zero at infinity faster than any polynomial ("rapid decay") (see [22]). In the case of approximate nodes, slightly weaker conditions are assumed, namely that the wavefunction is well behaved in the above sense in each nodal region and first-order smooth, i.e. the wavefunction has continuous first derivatives, at the nodes. The restricted variational space is linear, as a linear combination of such trial wavefunctions is still a wavefunction with the properties that are assumed above. Alternative to restricting the variational space, the Hamiltonian of interest, $\hat{H}=\hat{T}+\hat{V}$ (the kinetic part is $\hat{T}=-\frac{1}{2}\sum_{1\le i\le N}\nabla_i^2$, where $\nabla_i=\frac{\partial}{\partial r_{i,x}}+\frac{\partial}{\partial r_{i,y}}+\frac{\partial}{\partial r_{i,z}}$ is acting on the i-th electronic coordinates, and the

potential part is $\hat{V} = \sum_{1\le i<j\le N} \frac{1}{\left|\boldsymbol{r}_i - \boldsymbol{r}_j\right|} + \sum_{1\le i\le N} v\left(\boldsymbol{r}_i\right)$, where $v\left(\boldsymbol{r}\right)$ is the external potential), might be modified with the addition of delta function type infinite potential walls along the nodes. A replacement of $\hat{H}$ with such a modified Hamiltonian $\hat{H}'$ is an alternative way to ensure a nodal constraint on the trial wavefunctions upon energy minimization, as the eigenfunctions of $\hat{H}'$ naturally have nodes at the places where the potential of $\hat{H}'$ becomes infinite.

Appendix II

Here are the details for the derivation of Eq. (7).

$$
\begin{aligned}
&\left\langle g\Psi_k \middle| \hat{T} \middle| g\Psi_k \right\rangle - \left\langle g^2\Psi_k \middle| \hat{T} \middle| \Psi_k \right\rangle \\
&= -\frac{1}{2}\sum_{i=1}^{N}\sum_{\alpha=x,y,z} \left\langle g\Psi_k \middle| \frac{\partial^2}{\partial r_{i,\alpha}^2} \middle| g\Psi_k \right\rangle + \frac{1}{2}\sum_{i=1}^{N}\sum_{\alpha=x,y,z} \left\langle g^2\Psi_k \middle| \frac{\partial^2}{\partial r_{i,\alpha}^2} \middle| \Psi_k \right\rangle \\
&= \frac{1}{2}\sum_{i=1}^{N}\sum_{\alpha=x,y,z} \left\langle \frac{\partial\left(g\Psi_k\right)}{\partial r_{i,\alpha}} \middle| \frac{\partial\left(g\Psi_k\right)}{\partial r_{i,\alpha}} \right\rangle - \frac{1}{2}\sum_{i=1}^{N}\sum_{\alpha=x,y,z} \left\langle \frac{\partial\left(g^2\Psi_k\right)}{\partial r_{i,\alpha}} \middle| \frac{\partial\Psi_k}{\partial r_{i,\alpha}} \right\rangle \\
&= \frac{1}{2}\sum_{i=1}^{N}\sum_{\alpha=x,y,z} \left\langle \left(\frac{\partial g}{\partial r_{i,\alpha}}\right)\Psi_k + g\left(\frac{\partial\Psi_k}{\partial r_{i,\alpha}}\right) \middle| \left(\frac{\partial g}{\partial r_{i,\alpha}}\right)\Psi_k + g\left(\frac{\partial\Psi_k}{\partial r_{i,\alpha}}\right) \right\rangle \qquad \text{(II.1)} \\
&-\frac{1}{2}\sum_{i=1}^{N}\sum_{\alpha=x,y,z} \left\langle 2g\left(\frac{\partial g}{\partial r_{i,\alpha}}\right)\Psi_k + g^2\left(\frac{\partial\Psi_k}{\partial r_{i,\alpha}}\right) \middle| \frac{\partial\Psi_k}{\partial r_{i,\alpha}} \right\rangle \\
&= \frac{1}{2}\sum_{i=1}^{N}\sum_{\alpha=x,y,z} \left\langle \left(\frac{\partial g}{\partial r_{i,\alpha}}\right)\Psi_k \middle| \left(\frac{\partial g}{\partial r_{i,\alpha}}\right)\Psi_k \right\rangle = E_k + \frac{N_\uparrow}{2}\sum_{\alpha=x,y,z} \left\langle \left(\frac{\partial g}{\partial r_{N_\uparrow,\alpha}}\right)\Psi_k \middle| \left(\frac{\partial g}{\partial r_{N_\uparrow,\alpha}}\right)\Psi_k \right\rangle \\
&+\frac{N_\downarrow}{2}\sum_{\alpha=x,y,z} \left\langle \left(\frac{\partial g}{\partial r_{N_\uparrow+N_\downarrow,\alpha}}\right)\Psi_k \middle| \left(\frac{\partial g}{\partial r_{N_\uparrow+N_\downarrow,\alpha}}\right)\Psi_k \right\rangle
\end{aligned}
$$

The following arguments are used in Eq. (II.1): 1) integration by parts in the second equality, 2) derivative of a product in the third equality, 3) algebraic simplification in the fourth equality, and 4) coordinate interchange symmetry of $g(\boldsymbol{r}_1,\boldsymbol{r}_2,...,\boldsymbol{r}_N)$ in the last equality.

Appendix III

This appendix demonstrates that $g(\boldsymbol{r}_1,\boldsymbol{r}_2,...,\boldsymbol{r}_N)=\dfrac{\Psi^{(k)}(\boldsymbol{r}_1,\boldsymbol{r}_2,...,\boldsymbol{r}_N)}{\Psi_k(\boldsymbol{r}_1,\boldsymbol{r}_2,...,\boldsymbol{r}_N)}$ is finite, assuming both the eigenfunction $\Psi_k(\boldsymbol{r}_1,\boldsymbol{r}_2,...,\boldsymbol{r}_N)$ and the trial wavefunction $\Psi^{(k)}(\boldsymbol{r}_1,\boldsymbol{r}_2,...,\boldsymbol{r}_N)$ are analytic around the node.

An eigenfunction has 3N variables and its node, i.e. the positions in the 3N-dimensional space where the wavefunction is zero, is a hypersurface of dimension (3N-1). For each point on the nodal hypersurface there is a one-dimensional direction, perpendicular to the nodal hypersurface, that leads toward non-zero values, so the behavior of the eigenfunction, in the vicinity of its node, is effectively described by a one-dimensional Schrodinger equation:

$$\frac{d^2\Psi_k(r)}{dr^2}=f(r)\Psi_k(r), \tag{III.1}$$

where $f(r)=-2\left[E_k-V(r)\right]$. Subsequent differentiation of Eq. (III.1) gives

$$\frac{d^3\Psi_k(r)}{dr^3}=\frac{df(r)}{dr}\Psi_k(r)+f(r)\frac{d\Psi_k(r)}{dr}$$

$$\frac{d^4\Psi_k(r)}{dr^4}=\frac{d^2f(r)}{dr^2}\Psi_k(r)+2\frac{df(r)}{dr}\frac{d\Psi_k(r)}{dr}+f(r)\frac{d^2\Psi_k(r)}{dr^2} \tag{III.2}$$

…

Now, we employ a proof by contradiction. If $\left.\frac{d\Psi_k(r)}{dr}\right|_{r=0} = 0$ as well as $\Psi_k(0) = 0$, then Eqs. (III.1) and (III.2) dictate that all higher derivatives of the eigenfunction also vanish, i.e. $\left.\frac{d^n\Psi_k(r)}{dr^n}\right|_{r=0} = 0$ for any n. Based on the assumption that $\Psi_k(r)$ is analytic around the node at $r=0$, it follows that the eigenfunction identically vanishes everywhere around the origin, i.e. $\Psi_k(r) \equiv 0$, which is absurd. Consequently, $\Psi_k(0) = 0$ but $\left.\frac{d\Psi_k(r)}{dr}\right|_{r=0} \neq 0$. Hence, assuming the eigenfunction can be expanded in a Taylor series around the point at the node ($r=0$), $\Psi_k(r) = a_1 r + a_2 r^2 + a_3 r^3 + \ldots = r\left(a_1 + a_2 r + a_3 r^2 + \ldots\right)$, where $a_1 \neq 0$.

The Taylor expansion of a trial wavefunction around a point at the node has to be $\Psi^{(k)}(r) = b_n r^n + b_{n+1} r^{n+1} + b_{n+2} r^{n+2} + \ldots = r^n\left(b_n + b_{n+1} r + b_{n+2} r^2 + \ldots\right)$, where $b_n \neq 0$ and $n \geq 1$. The prefactor r^n guarantees the trial wavefunction $\Psi^{(k)}(r)$ vanishes at the node ($r=0$).

As a result, $\frac{\Psi^{(k)}(r)}{\Psi_k(r)} = \frac{r^n\left(b_n + b_{n+1} r + b_{n+2} r^2 + \ldots\right)}{r\left(a_1 + a_2 r + a_3 r^2 + \ldots\right)} = \frac{r^{n-1}\left(b_n + b_{n+1} r + b_{n+2} r^2 + \ldots\right)}{a_1 + a_2 r + a_3 r^2 + \ldots}$ does not diverge at the node of the eigenfunction.

Appendix IV

Lemma: The minimizing wavefunction $\tilde{\Psi}^{(k)}_{\min}$ is antisymmetric. (The spin-free wave functions that are antisymmetric are such with respect to the interchange of electron coordinates that correspond to the same spin.)

Proof: Define Φ to be the normalized antisymmetric wavefunction such that the nodes of Φ divide the N-electron configuration space into m nodal regions $\tilde{L}_j$ $\left(j = 1,2,\ldots,m\right)$. The nodes of the trial wavefunctions $\tilde{\Psi}^{(k)}$ are assumed to be the nodes of Φ.

Choose a point $\vec{R}=\left(\vec{r}_1,\vec{r}_2,\ldots,\vec{r}_N\right)$ in the whole configuration space of N electrons. Label the nodal region, where the point $\vec{R}$ lies, as A. An interchange of two electrons having the same spin, say the first and the second electrons, maps the point $\vec{R}$ to a new point $\vec{R}'=\left(\vec{r}_2,\vec{r}_1,\ldots,\vec{r}_N\right)$. Label the nodal region, where the point $\vec{R}'$ lies, as A'.

The nodal regions A and A' are different, because $\Phi\left(\vec{r}_1,\vec{r}_2,\ldots,\vec{r}_N\right)$ and $\Phi\left(\vec{r}_2,\vec{r}_1,\ldots,\vec{r}_N\right)$ have different signs (as a reminder: Φ is antisymmetric). If $\vec{R}$ and $\vec{R}'$ are connected with a straight line, there has to be an odd number of nodal crossings along the line as there is a sign change at each nodal crossing.

The interchange of the first and second electrons, in fact, maps every point of A to a point of A' making the two nodal regions "isomorphic", i.e. of the same form and size. Since the nodal regions A and A' are isomorphic, the ground state in A is mapped to the ground state in A' (up to a normalization factor) by the interchange of the first and second electrons. In the same manner, another nodal region, say B, is mapped to an isomorphic nodal region B', C to C', D to D' and so on. That is, one half of the configuration space (A, B, C, D, …) is mapped to its isomorphic other half (A', B', C', D', …). The uncertainty in the normalization factor of the ground state is reduced to just an uncertainty in the sign due to the perfect mirror symmetry between the two isomorphic halves.

The minimizing wavefunction $\tilde{\Psi}^{(k)}_{\min}$ is a ground state within each nodal region. As a result, $\tilde{\Psi}^{(k)}_{\min}$ restricted to A is mapped (up to a sign) to $\tilde{\Psi}^{(k)}_{\min}$ restricted to A' by the interchange of the first and second electrons, i.e. $\tilde{\Psi}^{(k)}_{\min}\left(\vec{r}_1,\vec{r}_2,\ldots,\vec{r}_N\right)=\pm\tilde{\Psi}^{(k)}_{\min}\left(\vec{r}_2,\vec{r}_1,\ldots,\vec{r}_N\right)$.

On the one hand, every minimizing wavefunction, antisymmetric or not, changes sign across a node because it is linear around the node (Appendix III). On the other hand, as stated above, there is an odd number of nodal crossings along the straight line connecting $\vec{R}$ and $\vec{R}'$. Finally, $\tilde{\Psi}^{(k)}_{\min}\left(\vec{r}_1,\vec{r}_2,\ldots,\vec{r}_N\right)=-\tilde{\Psi}^{(k)}_{\min}\left(\vec{r}_2,\vec{r}_1,\ldots,\vec{r}_N\right)$.

Appendix V

Tables V.1-V.4 present, in Hartrees, the energies and corresponding errors of the minimizing wavefunctions in single, double, triple, and quadruple combinations of nodal regions for four 4S state wavefunctions of the hydrogen atom with approximate nodes.

Nodal regions	$\tilde{E}_{\min}^{(k)}$	$\left[E_k - \tilde{E}_{\min}^{(k)}\right]^2$ with $\tilde{E}_{\min}^{(k)}$ over the nodal regions	Eq. (10) with $\tilde{E}_{\min}^{(k)}$ over 1,2,3,4	Eq. (10) with $\tilde{E}_{\min}^{(k)}$ over the nodal regions
1	-0.14010	$1.1849*10^{-2}$	$1.1819*10^{-2}$	0.
2	-0.01000	$4.5153*10^{-4}$	$4.5743*10^{-4}$	0.
3	-0.03261	$1.8427*10^{-6}$	$1.4862*10^{-6}$	0.
4	-0.03106	$3.7671*10^{-8}$	$1.1052*10^{-7}$	0.
1,2	-0.03453	$1.0764*10^{-5}$	$2.5995*10^{-3}$	$2.5897*10^{-3}$
1,3	-0.03829	$4.9508*10^{-5}$	$6.2577*10^{-4}$	$5.7819*10^{-4}$
1,4	-0.03199	$5.4590*10^{-7}$	$1.0122*10^{-4}$	$1.0086*10^{-4}$
2,3	-0.02823	$9.1122*10^{-6}$	$8.9746*10^{-5}$	$7.9779*10^{-5}$
2,4	-0.03030	$8.9878*10^{-7}$	$1.6486*10^{-5}$	$1.5306*10^{-5}$
3,4	-0.03126	$1.9032*10^{-10}$	$2.9484*10^{-7}$	$2.7933*10^{-7}$
1,2,3	-0.03305	$3.2276*10^{-6}$	$5.9458*10^{-4}$	$5.9184*10^{-4}$
1,2,4	-0.03121	$1.7651*10^{-9}$	$1.1387*10^{-4}$	$1.1384*10^{-4}$
1,3,4	-0.03207	$6.7424*10^{-7}$	$8.7959*10^{-5}$	$8.7493*10^{-5}$
2,3,4	-0.03060	$4.2089*10^{-7}$	$1.4539*10^{-5}$	$1.3920*10^{-5}$
1,2,3,4	-0.03139	$1.9140*10^{-8}$	$1.0167*10^{-4}$	$1.0167*10^{-4}$

Table V.1. The energies and corresponding errors of the wavefunction V.1 for the 4S state of the hydrogen atom with approximate nodes. The energies are in Hartrees. The squared norms of the wavefunction in the four nodal regions are respectively 0.007188, 0.030936, 0.128878, 0.832998.

Nodal regions	$\tilde{E}^{(k)}_{\min}$	$\left[E_k - \tilde{E}^{(k)}_{\min}\right]^2$ with $\tilde{E}^{(k)}_{\min}$ over the nodal regions	Eq. (10) with $\tilde{E}^{(k)}_{\min}$ over 1,2,3,4	Eq. (10) with $\tilde{E}^{(k)}_{\min}$ over the nodal regions
1	-0.01000	$4.5153*10^{-4}$	$4.5442*10^{-4}$	0.
2	-0.04337	$1.4700*10^{-4}$	$1.4536*10^{-4}$	0.
3	-0.02636	$2.3944*10^{-5}$	$2.4611*10^{-5}$	0.
4	-0.03153	$8.1424*10^{-8}$	$4.7355*10^{-8}$	0.
1,2	-0.03998	$7.6272*10^{-5}$	$1.7676*10^{-4}$	$1.0167*10^{-4}$
1,3	-0.02580	$2.9677*10^{-5}$	$3.9181*10^{-5}$	$8.7611*10^{-6}$
1,4	-0.03145	$4.0860*10^{-8}$	$1.8031*10^{-6}$	$1.7850*10^{-6}$
2,3	-0.03039	$7.4593*10^{-7}$	$5.3203*10^{-5}$	$5.2335*10^{-5}$
2,4	-0.03193	$4.5963*10^{-7}$	$4.8663*10^{-6}$	$4.4939*10^{-6}$
3,4	-0.03102	$5.2981*10^{-8}$	$2.4927*10^{-6}$	$2.4039*10^{-6}$
1,2,3	-0.02985	$1.9470*10^{-6}$	$6.3667*10^{-5}$	$6.1526*10^{-5}$
1,2,4	-0.03185	$3.5525*10^{-7}$	$6.5460*10^{-6}$	$6.2670*10^{-6}$
1,3,4	-0.03095	$9.2014*10^{-8}$	$4.0657*10^{-6}$	$3.9280*10^{-6}$
2,3,4	-0.03139	$1.9591*10^{-8}$	$6.7730*10^{-6}$	$6.7678*10^{-6}$
1,2,3,4	-0.03138	$4.5884*10^{-9}$	$9.4020*10^{-6}$	$9.4020*10^{-6}$

Table V.2. The energies and corresponding errors of the first alternative wavefunction V.2 for the 4S state of the hydrogen atom with approximate nodes. The energies are in Hartrees. The squared norms of the wavefunction in the four nodal regions are respectively 0.003377, 0.029859, 0.096241, 0.870523.

Nodal regions	$\tilde{E}_{\min}^{(k)}$	$\left[E_k - \tilde{E}_{\min}^{(k)}\right]^2$ with $\tilde{E}_{\min}^{(k)}$ over the nodal regions	Eq. (10) with $\tilde{E}_{\min}^{(k)}$ over 1,2,3,4	Eq. (10) with $\tilde{E}_{\min}^{(k)}$ over the nodal regions
1	-0.02075	$1.1023*10^{-4}$	$1.1123*10^{-4}$	0.
2	-0.03789	$4.4137*10^{-5}$	$4.3511*10^{-5}$	0.
3	-0.02588	$2.8840*10^{-5}$	$2.9350*10^{-5}$	0.
4	-0.03178	$2.7825*10^{-7}$	$2.3057*10^{-7}$	0.
1,2	-0.03559	$1.8868*10^{-5}$	$5.2595*10^{-5}$	$3.4136*10^{-5}$
1,3	-0.02562	$3.1680*10^{-5}$	$3.3473*10^{-5}$	$1.2577*10^{-6}$
1,4	-0.03170	$2.0479*10^{-7}$	$9.8504*10^{-7}$	$8.2084*10^{-7}$
2,3	-0.02894	$5.3250*10^{-6}$	$3.2960*10^{-5}$	$2.7415*10^{-5}$
2,4	-0.03204	$6.1811*10^{-7}$	$2.0613*10^{-6}$	$1.5154*10^{-6}$
3,4	-0.03110	$2.1550*10^{-8}$	$3.5598*10^{-6}$	$3.5221*10^{-6}$
1,2,3	-0.02863	$6.8585*10^{-6}$	$3.5934*10^{-5}$	$2.8826*10^{-5}$
1,2,4	-0.03196	$5.0796*10^{-7}$	$2.7722*10^{-6}$	$2.3294*10^{-6}$
1,3,4	-0.03104	$4.3752*10^{-8}$	$4.2085*10^{-6}$	$4.1427*10^{-6}$
2,3,4	-0.03136	$1.1844*10^{-8}$	$5.0638*10^{-6}$	$5.0600*10^{-6}$
1,2,3,4	-0.03130	$2.2384*10^{-9}$	$7.2620*10^{-6}$	$7.2620*10^{-6}$

Table V.3. The energies and corresponding errors of the second alternative wavefunction V.3 for the 4S state of the hydrogen atom with approximate nodes. The energies are in Hartrees. The squared norms of the wavefunction in the four nodal regions are respectively 0.005799, 0.037427, 0.109387, 0.847386.

Nodal regions	$\tilde{E}_{\min}^{(k)}$	$\left[E_k - \tilde{E}_{\min}^{(k)}\right]^2$ with $\tilde{E}_{\min}^{(k)}$ over the nodal regions	Eq. (10) with $\tilde{E}_{\min}^{(k)}$ over 1,2,3,4	Eq. (10) with $\tilde{E}_{\min}^{(k)}$ over the nodal regions
1	-0.01000	$4.5153*10^{-4}$	$5.7794*10^{-4}$	0.
2	-0.05227	$4.4195*10^{-4}$	$3.3239*10^{-4}$	0.
3	-0.03312	$3.4957*10^{-6}$	$8.4886*10^{-7}$	0.
4	-0.03178	$2.7835*10^{-7}$	$5.1235*10^{-6}$	0.
1,2	-0.04941	$3.2965*10^{-4}$	$3.4904*10^{-4}$	$1.1295*10^{-4}$
1,3	-0.03242	$1.3758*10^{-6}$	$1.8240*10^{-5}$	$1.5622*10^{-5}$
1,4	-0.03153	$7.8434*10^{-8}$	$1.1632*10^{-5}$	$5.3270*10^{-6}$
2,3	-0.03885	$5.7797*10^{-5}$	$1.0008*10^{-4}$	$7.6934*10^{-5}$
2,4	-0.03457	$1.1048*10^{-5}$	$4.9776*10^{-5}$	$4.9492*10^{-5}$
3,4	-0.03214	$7.9189*10^{-7}$	$3.9694*10^{-6}$	$3.5507*10^{-7}$
1,2,3	-0.03824	$4.8828*10^{-5}$	$1.1027*10^{-4}$	$9.2654*10^{-5}$
1,2,4	-0.03433	$9.5012*10^{-6}$	$5.4966*10^{-5}$	$5.4882*10^{-5}$
1,3,4	-0.03196	$4.9800*10^{-7}$	$8.7447*10^{-6}$	$4.3961*10^{-6}$
2,3,4	-0.03422	$8.8319*10^{-6}$	$3.7932*10^{-5}$	$3.7899*10^{-5}$
1,2,3,4	-0.03404	$7.7898*10^{-6}$	$2.8065*10^{-5}$	$2.8065*10^{-5}$

Table V.4. The energies and corresponding errors of the third alternative wavefunction V.4 for the 4S state of the hydrogen atom with approximate nodes. The energies are in Hartrees. The squared norms of the wavefunction in the four nodal regions are respectively 0.007466, 0.102640, 0.240274, 0.649620.

Appendix VI

In addition to the exact and approximate wavefunctions for the 4S state of the hydrogen atom, consider also the exact and two approximate fifth excited states of the one-dimensional harmonic oscillator[††] (Fig. VI.1) [23].

Table VI.1 summarizes the energy and error expression values of the minimizing wavefunctions with nodal approximations both in the entire space and in selected nodal regions only. It becomes clear that a restriction of HO-1 to the third nodal region and of HO-2 to the first nodal region improves the energy estimates.

[††] The two wavefunctions that minimize the energy-expectation value of the harmonic oscillator, while being constrained to nodes displaced from the exact positions, are abbreviated HO-1 and HO-2 (see the caption of Fig. VI.1 for more details).

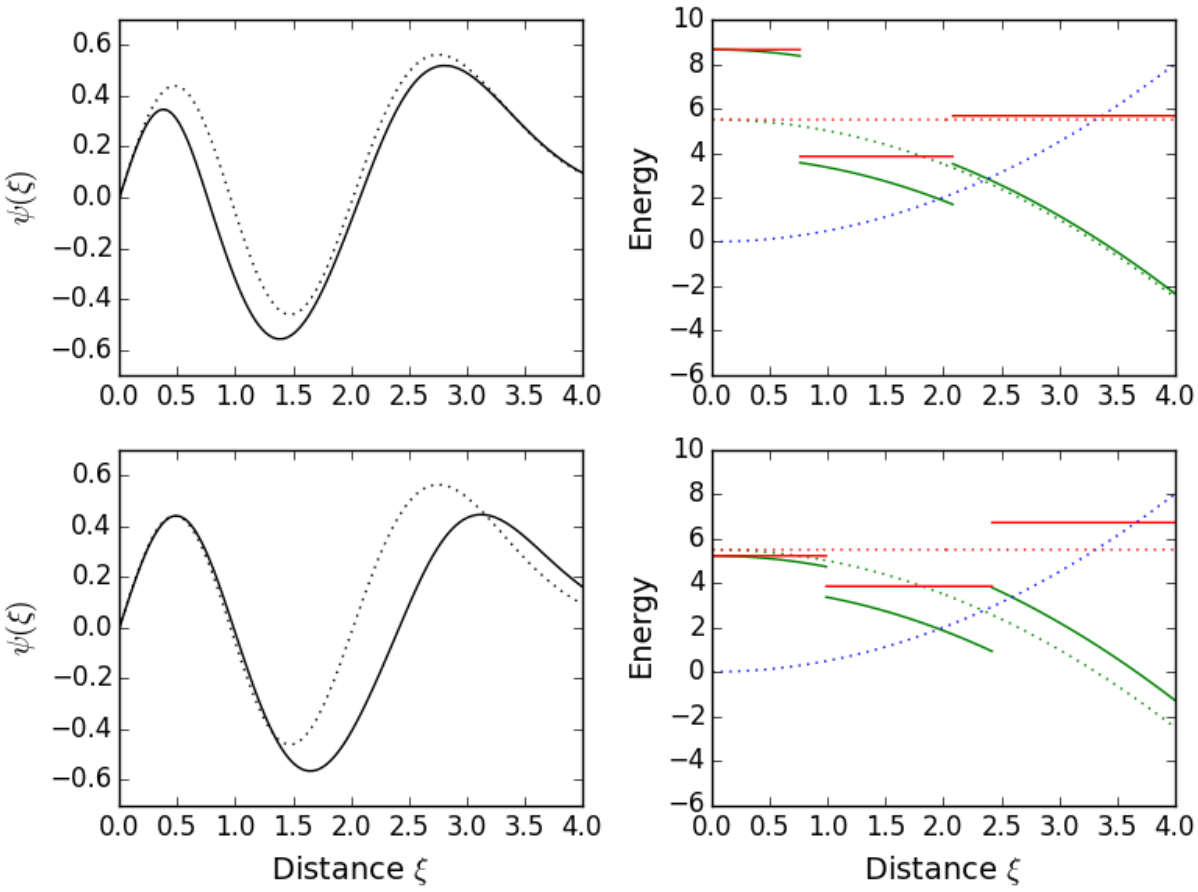

Fig. VI.1 The exact (dotted lines) and approximate (solid lines) wavefunctions corresponding to the fifth excited state of the harmonic oscillator (HO) are depicted on the left-hand side of the figure. The exact wavefunction (upper and lower left) has nodes at 0.959 and 2.020, while the first approximate wavefunction (HO-1, upper left) has nodes at 0.759 and 2.080 and the second approximate wavefunction (HO-2, lower left) has nodes at 0.985 and 2.420. The exact energy of HO is 5.5000, while the nodal-region energies of the HO-1 are 8.6564, 3.8478, and 5.6742 and the nodal-region energies of HO-2 are 5.2218, 3.8525, and 6.7234. The corresponding local energies are depicted on the right-hand side of the figure. The kinetic components are in green (curves with decreasing values), the potential components are in blue (curves with increasing values) and the sum of the two is in red (horizontal lines). Only the right halves of the wavefunctions are shown due to the antisymmetry with respect to the origin. A representation of the harmonic-oscillator problem with unitless distance and energy is chosen [24].

Approximate wavefunction	Energy	Error expression 1, Eq. (10)	Error expression 2, Eq. (12) [29]
HO-1 (1, 2, 3)	5.1974	1.9478	4.6713
HO-1 (3)	5.6742	0.2273	0.2273
HO-2 (1, 2, 3)	5.1319	1.6451	1.3926
HO-2 (1)	5.2218	0.0081	0.0081

Table VI.1. The energies and error-expression evaluations of the approximate wavefunctions (HO-1 and HO-2 as defined previously) are shown in the table. The nodal regions, where the wavefunctions are considered, are indicated in the leftmost column (in parentheses). The harmonic oscillator energies are unitless.

References:

1. E. Hylleraas and B. Undheim, *Z. Phys*. **65**, 759 (1930); J. K. L. McDonald, *Phys. Rev*. **43**, 830 (1933).
2. R. Courant and D. Hilbert, *Methods of Mathematical Physics*, 1st English ed. (Interscience, New York, 1953).
3. J. O. Hirshfeld, C. J. Goebel, and L. W. Bruch, J. Chem. Phys. **61**, 5456 (1974); E. B. Wilson, J. Chem. Phys. **63**, 4870 (1975); G. Hunter, Int. J. Quantum Chem. **19**, 755 (1981).
4. P. J. Reynolds, D. Ceperley, B. J. Alder, and W. A. Lester, Jr., J. Chem. Phys. **77**, 5593 (1982).
5. D. Ceperley, J. Stat. Phys. **63**, 1237 (1991).
6. W. M. C. Foulkes, R. Q. Hood, and R. J. Needs, Phys. Rev. B **60**, 4558 (1999).
7. P. G. Hipes, Phys. Rev. B **83**, 195118 (2011).
8. M. Bajdich, L. Mitas, G. Drobny, and L. K. Wagner, Phys. Rev. B **72**, 075131 (2005).
9. L. Mitas, Phys. Rev. Lett. **96**, 240402 (2006).
10. J. S. Briggs and M. Walter, Phys. Rev. A **74**, 062108 (2006).
11. D. Bressanini and P. J. Reynolds, Phys. Rev. E **84**, 046705 (2011).
12. A. J. Williamson, J. C. Grossman, R. Q. Hood, A. Puzder, and G. Galli, Phys. Rev. Lett. **89**, 196803 (2002); J. E. Vincent, J. Kim, and R. M. Martin, Phys. Rev. B 75, 045302 (2007).
13. J. Yu, L. K. Wagner, and E. Ertekin, J. Chem. Phys. **143**, 224707 (2015).
14. R. Q. Hood, P. R. C Kent, R. J. Needs, and P. R. Briddon, Phys. Rev. Lett. **91**, 076403 (2003).

15. F. Marsusi, J. Sabbaghzadeh, and N. D. Drummond, Phys. Rev. B **84**, 245315 (2011).
16. A. Ghosal, A. D. Guclu, C. J. Umrigar, D. Ullmo, and H. U. Baranger, Phys. Rev. B **76**, 085341 (2007); S. A. Blundell and S. Chacko, Phys. Rev. B **83**, 195444 (2011).
17. N. D. Drummond and R. J. Needs, Phys. Rev. B **87**, 045131 (2013).
18. T. Bouabca, N. B. Amor, D. Maynau, and M. Caffarel, J. Chem. Phys. **130**, 114107 (2009); N. Dupuy, S. Bouaouli, F. Mauri, S. Sorella, and M. Casula, J. Chem. Phys. **142**, 214109 (2015); R. Guareschi, H. Zulfikri, C. Dabay, F. M. Floris, C. Amovilli, B. Mennucci, and C. Filippi, J. Chem. Theory Comput. (ASAP).
19. A. S. Petit, B. A. Wellen, and A. B. McCoy, J. Chem. Phys **138**, 034105 (2013); R. C. Fortenberry, Q. Yu, J. S. Mancini, J. M. Bowman, T. J. Lee, T. Daniel Crawford, W. F. Klemperer, and J. S. Francisco, J. Chem. Phys. **143**, 071102 (2015); J. E. Ford and A. B. McCoy, Chem. Phys. Lett. **645**, 15 (2016).
20. C.-J. Huang, C. Filippi, and C. Umrigar, J. Chem. Phys. **108**, 8838 (1998).
21. R. McWeeny, "Methods of Molecular Quantum Mechanics", Academic Press (1989).
22. R. D. Richtmeyer, "Principles of Advanced Mathematical Physics", Vol. I, Springer-Verlag (1978).
23. The numerical calculations are done by modified versions of harmonic1.f90 and hydrogen_radial.f90 from [24].
24. P. Giannozzi, Lecture notes in "Numerical Methods in Quantum Mechanics", http://www.fisica.uniud.it/~giannozz/Corsi/MQ/mq.html.
25. C. J. Umrigar, K. G. Wilson, and J. W. Wilkins, Phys. Rev. Lett. **60**, 1719 (1988).
26. P. R. C. Kent, R. J. Needs, and G. Rajagopal, Phys. Rev. B **59,** 12344 (1999).
27. J. H. Bartlett, Phys. Rev. **98**, 1067 (1955).
28. F. A. Reboredo and P. R. C. Kent, Phys. Rev. B **77**, 245110 (2008).
29. M. Dubecky, R. Derian, L. Mitas, and I. Stich, J. Chem. Phys. **133**, 244301 (2010).
30. Expression $\frac{1}{M}\sum_{n=1}^{M}\left[\frac{\left\langle g_n\tilde{\Psi}_{\min}^{(k)}\middle|\hat{H}\middle|\tilde{\Psi}_{\min}^{(k)}\right\rangle}{\left\langle g_n\tilde{\Psi}_{\min}^{(k)}\middle|\tilde{\Psi}_{\min}^{(k)}\right\rangle}-\left\langle\tilde{\Psi}_{\min}^{(k)}\middle|\hat{H}\middle|\tilde{\Psi}_{\min}^{(k)}\right\rangle\right]^2$ is used as a substitute for expression (12), which employs all possible scaling functions. The M scaling functions are of the form $g=e^{-2d\left(x-x_0\right)^2}$. The parameters for the hydrogen atom example are (M=4): d_1=12.3251, $x_{0,1}$=0.9358; d_2=1.9222, $x_{0,2}$=4.2412; d_3=0.3527, $x_{0,3}$=11.0644; d_4=0.0104, $x_{0,4}$=47.7590, while the ones for the two harmonic oscillator examples are (M=3): d_1=46.9440, $x_{0,1}$=0.4795; d_2=38.3518, $x_{0,2}$=1.4895; d_3=1.7408, $x_{0,3}$=4.510.
31. T. C. Scott, A. Luchow, D. Bressanini, J. D. Morgan III, Phys. Rev. A 75, 060101(R) (2007).